Landslides (2026) 23:1561–1580
DOI 10.1007/s10346-026-02720-1
Received: 3 October 2025
Accepted: 5 February 2026
Published online: 21 March 2026

E. B. Masi · F. Caleca · P. Confuorto · V. Tofani · N. Casagli

Shallow landslides in Tuscany (Central Italy) triggered by the November 2023 heavy rainfall event

Abstract On 2 November 2023, an extreme rainfall event struck Tuscany (central Italy), causing severe floods and triggering widespread landslides, which resulted in 8 fatalities, 300 evacuees, and an estimated economic loss of 2 billion. The intensification in recent years of these extreme rainfall events in Italy, driven by the ongoing climate change, has led to a significant increase in the occurrence of shallow landslides, posing growing threats to both infrastructure and communities. The development of detailed event-based landslide inventories represents a fundamental step in the perspective of climate change adaptation, being essential for emergency response, hazard assessment, and long-term risk mitigation. Integrating field surveys, high-resolution satellite imagery, and NDVI-based change detection analyses, 411 shallow landslides triggered during the event were identified, ranging in extension from a minimum of a few square meters to a maximum of 8,000 m^2. 120 buildings were impacted, along with approximately 21.6 km of roads, with the most affected segments belonging to local and municipal networks, underscoring the vulnerability of secondary infrastructure. Spatial distribution of landslides was studied considering patterns of rainfall and predisposing factors. The results highlight that areas with moderate infiltration capacity, intermediate slope angles, moderate clay content, land uses featuring limited rainfall interception, and weak root reinforcement are especially susceptible to shallow landslides triggered by intense rainfall. This study provides event-based insights into rainfall-induced shallow landslides under extreme hydro-meteorological conditions, contributing to the understanding of their occurrence patterns and supporting susceptibility assessment, early warning activities, and climate-resilient land-use planning.

Keywords Shallow landslides · Landslide susceptibility · Landslide inventory · Predisposing factors · Climate change · Forecasting models

Introduction

Tuscany (central Italy) experienced an extreme rainfall event on 2 November 2023 that caused severe flooding and widespread landslides, resulting in eight fatalities, approximately 300 evacuees, and estimated economic losses of around 2 billion euros (Agnoletti et al. 2023, ANSA 2024). This event is part of a broader trend of increasing frequency and intensity of extreme precipitation events across Italy and Europe, driven by ongoing climate change (Valkaniotis et al. 2022; Diakakis et al. 2023; Kushabaha et al. 2024). Such intensification has led to a significant rise in shallow landslide occurrences, which pose growing threats to infrastructure and communities. Hydrologically induced natural hazards, including shallow landslides, have indeed caused increasing damage worldwide in recent years (Froude and Petley 2018; Swiss Re 2019; Emberson et al. 2020) and this escalation is mainly due to two converging factors: expansion of urban development into hazard-prone areas and more frequent intense rainfall events.

Accurate and detailed inventories of landslide events are essential tools for understanding distribution, controlling factors, and impacts of these phenomena, in the perspective of supporting emergency response, hazard assessment, and long-term risk mitigation strategies. The prompt compilation of landslide inventories following extreme rainfall provides indeed essential knowledge for susceptibility analyses and calibration/validation of predictive models (Guzzetti et al. 2012; Smith et al. 2021). Predictive models can rely nowadays on different approaches (statistical, machine learning, physically based modeling) highly developed and efficiently supported by advanced and powerful computers, but very often the lack of complete and robust landslide databases—essential for their calibration and validation- extremely limits their potential (e.i. Salvatici et al. 2018; Masi et al. 2023).

Numerous recent case studies have highlighted the relevance of post-event inventories: e.g. Sicily, Italy (Mondini et al. 2011); Emilia-Romagna, Italy (Ferrario and Livio 2023; Berti et al. 2025); Marche, Italy (Confuorto et al. 2025); Austrian Alps, Austria (Dietrich and Krautblatter 2017), the Pyrenees (Hürlimann et al. 2022), eastern China (Zeng et al. 2023), and Puerto Rico (Ramos-Scharrón et al. 2022).

Over the past decades, landslide inventory methods have evolved significantly. Conventional ground-based surveys (Pellicani and Spilotro 2015; Lazzari et al. 2018; Santangelo et al. 2023) remain fundamental for detailed site characterization, yet they are increasingly supplemented—and in some cases replaced—by remote sensing technologies. Aerial and satellite image interpretation (Hölbling et al. 2017; Del Soldato et al. 2018), enhanced by the integration of Digital Elevation Models (Lazzari et al. 2018; Pawluszek 2019), now enables wide-area mapping with unprecedented spatial and temporal resolution. Recently, artificial intelligence and machine learning techniques have introduced automated and semi-automated approaches for landslide detection using optical and radar datasets (Plank et al. 2016; Mondini et al. 2019; Catani 2021; Su et al. 2021; Meena et al. 2022), offering scalable solutions for large-scale monitoring.

In a context of changing precipitation regimes, with short-term extreme events currently difficult to predict that increasingly recur, such as Tuscany, analyzing landslides triggered by each extreme and widespread rainfall event is essential for understanding evolving hazard dynamics. In Tuscany, as well as in other regions of Italy, indeed, extreme and extensive rainfall events currently occur with an annual (at least) frequency (Confuorto et al. 2025; Ferrario and Livio 2023; Gozzini et al. 2022; Davolio et al. 2020).

This study investigated the landslides triggered by the November 2023 extreme rainfall in Tuscany. First, a comprehensive inventory of landslides was constructed by means of a multi-source approach based on the use of high-resolution multispectral optical satellite imagery and field surveys. The satellite imagery (acquired before and after the event) allowed for the detection of surface changes related to landslide activation, such as vegetation loss, debris deposits, and freshly exposed material, through change detection analyses and visual geomorphological interpretation. The remote sensing analysis was complemented by extensive field surveys ensuring the robustness and completeness of the inventory. The spatial pattern of landslides was then analyzed in relation to rainfall distribution and a suite of predisposing factors including topography, lithology, soil properties, and land use.

Landslide events

Study area

The study area is located in northern Tuscany (region of central Italy), and it is delimited by the borders of the municipalities affected by shallow landslides during the rainfall event of 2 November 2023 (Fig. 1).

Tuscany region encompasses an area of approximately 23,000 km^2 and exhibits a highly diversified landscape, transitioning from coastal plains and major river valleys to hilly and mountainous terrains further inland. The highest elevations are found in the northeastern sector, where the Northern Apennines constitute the principal mountain chain. Topographically, hills cover about two-thirds of the territory, while mountainous areas represent roughly 20%, and plains and valleys account for the remaining 10%.

From a geological perspective, the northeastern portion of Tuscany is dominated by the Northern Apennine, which developed during the Upper Cretaceous period following the tectonic collision between the Corso-Sardinian block and the Adria microplate. This orogenic process resulted in a complex thrust-nappe structure and the propagation of fault systems, which contributed to the formation of the present-day ridges and depressions setting (Vai 2001; Bartolini 2003; Bortolotti 1992; Elter et al. 1975; Carmignani and Kligfield 1990). The region's lithology is characterized by flysch facies composed of sandstone and calcareous marls in the northwestern areas, with similar lithological compositions extending into the central and southern zones, alongside extensive deposits of colluvial and alluvial sediments.

The climate of Tuscany is highly variable due to its complex topography and geographical setting, influenced by latitude, altitude, and proximity to the sea and mountain ranges. Precipitation shows strong spatial variability, with the northern areas (Apuan Alps, northern Apennines, and surrounding areas) among the wettest in Italy receiving over 2000 mm annually, while southern coastal and island zones record less than 600 mm (Gozzini et al. 2022).

In recent decades, the region has undergone significant climatic changes, including an average temperature increase of approximately 1.7 °C since the mid-twentieth century, with sharper trends

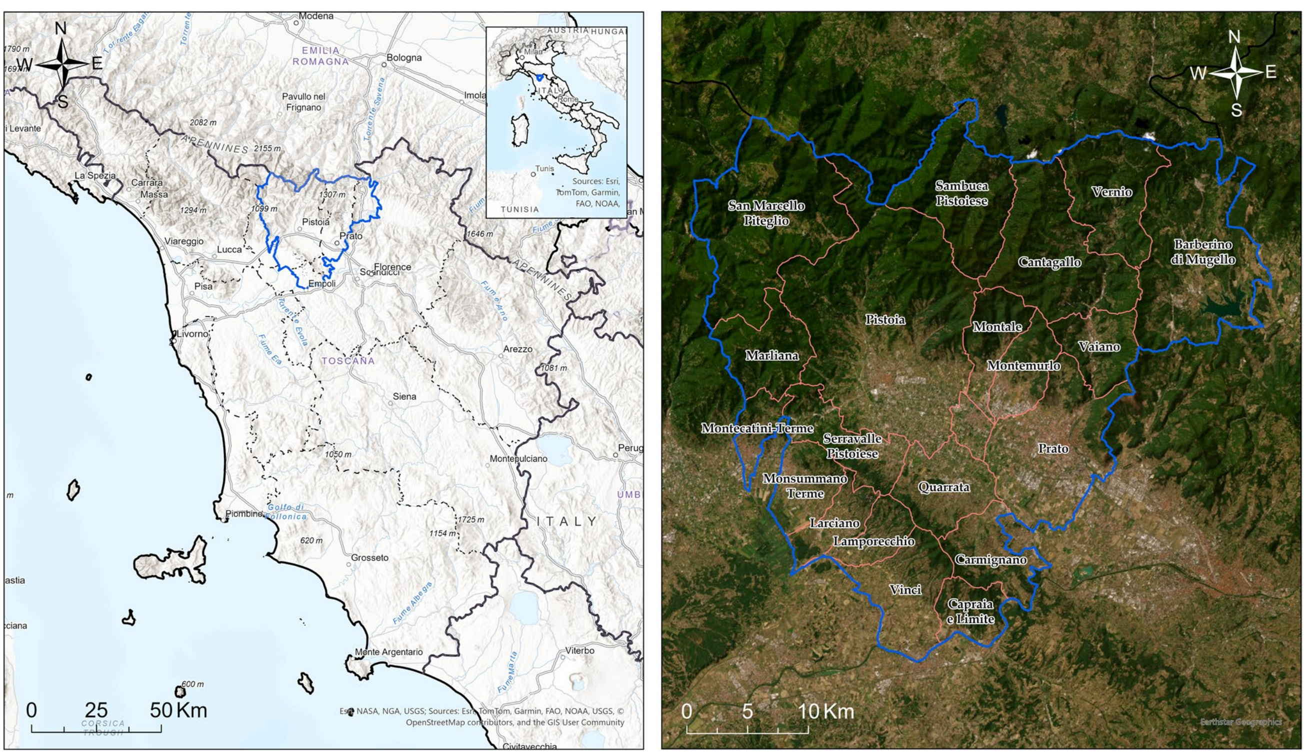

Fig. 1 Study area (in blue). Administrative divisions: in red municipalities affected by landslides; provinces in dotted black; regions in solid black

in spring and summer (Bartolini et al. 2011). These changes are accompanied by a rise in the frequency and intensity of extreme events, such as heatwaves and short-duration heavy rainfall (Bartolini et al. 2008, 2014). Notably, several urban areas have experienced increases in precipitation extremes, reflecting a shift toward more localized and intense hydrometeorological hazards, with implications for slope stability, erosion processes, and hydrogeological risk (Gozzini et al. 2022; Bartolini et al. 2014).

The study area specifically covers approximately 1293 km^2 between 43°8′19″ and 43°43′20″ N latitude and 10°42′58″ and 11°18′47″ E longitude. It includes most of the Provinces of Pistoia and Prato, with parts of the metropolitan area of Florence, covering 20 municipalities (Barberino di Mugello, Cantagallo, Capraia e Limite, Carmignano Lamporecchio, Larciano, Marliana, Monsummano Terme, Montale, Montecatini-Terme, Montemurlo, Prato, Quarrata, Sambuca Pistoiese, San Marcello Piteglio, Serravalle Pistoiese, Vaiano, Vernio and Vinci). The northern part is occupied by reliefs belonging to the Northern Apennine with elevations up to approximately 1000 m a.s.l. The central-southeastern part is dominated by the highly urbanized plain of Pistoia-Prato, while in the southwestern portion, the hills of the sub-Apennine ridge of Montalbano border the plain of Vinci, Lamporecchio and Larciano. The Ombrone Pistoiese and Bisenzio rivers are the main hydrological axes, flowing southward and converging near the Arno River (main river of Tuscany), they have shaped wide alluvial plains where urban and agricultural developments are concentrated.

The study area is characterized by the presence of both consolidated and unconsolidated deposits, including marine sedimentary rocks such as marl, sandstone, and limestone associated with the Tuscan Nappe and Ligurian complexes (Fig. 2). These are locally overlain by Quaternary fluvio-lacustrine sequences deposited in tectonically controlled intermontane basins. Additionally, the area includes Holocene alluvial fans, terraced fluvial deposits, colluvial accumulations, and landslide bodies. Isolated Pliocene marine sediments also occur, marking former transgressive phases. From a lithological-lithotechnical standpoint, the study area includes a variety of materials ranging from weak to very weak rock masses—with both regular and irregular discontinuities—to heterometric or massive-textured units without discontinuities (Fig. 2). It also features medium to good-quality lithified rock masses, either with persistent discontinuities or massive textures, as well as fine-grained soils and medium- to coarse-grained soils.

Rainfall event

On November 2nd, Tuscany was affected by an intense Atlantic weather disturbance that brought locally exceptional amounts of rainfall (Fig. 3). During the afternoon, the transit of an instability line preceding the cold front favored the development of a thunderstorm line that remained nearly stationary for 5–6 h (from about 4:30 PM to 9:30 PM). This line has interested northern Tuscany, extending from the provinces of Livorno and Pisa to the Mugello area, passing through the Lower Arno Valley, the southern areas of the province of Pistoia, the Montalbano area, and the province of Prato. The event was likely caused by the convergence of strong southerly winds over the southern

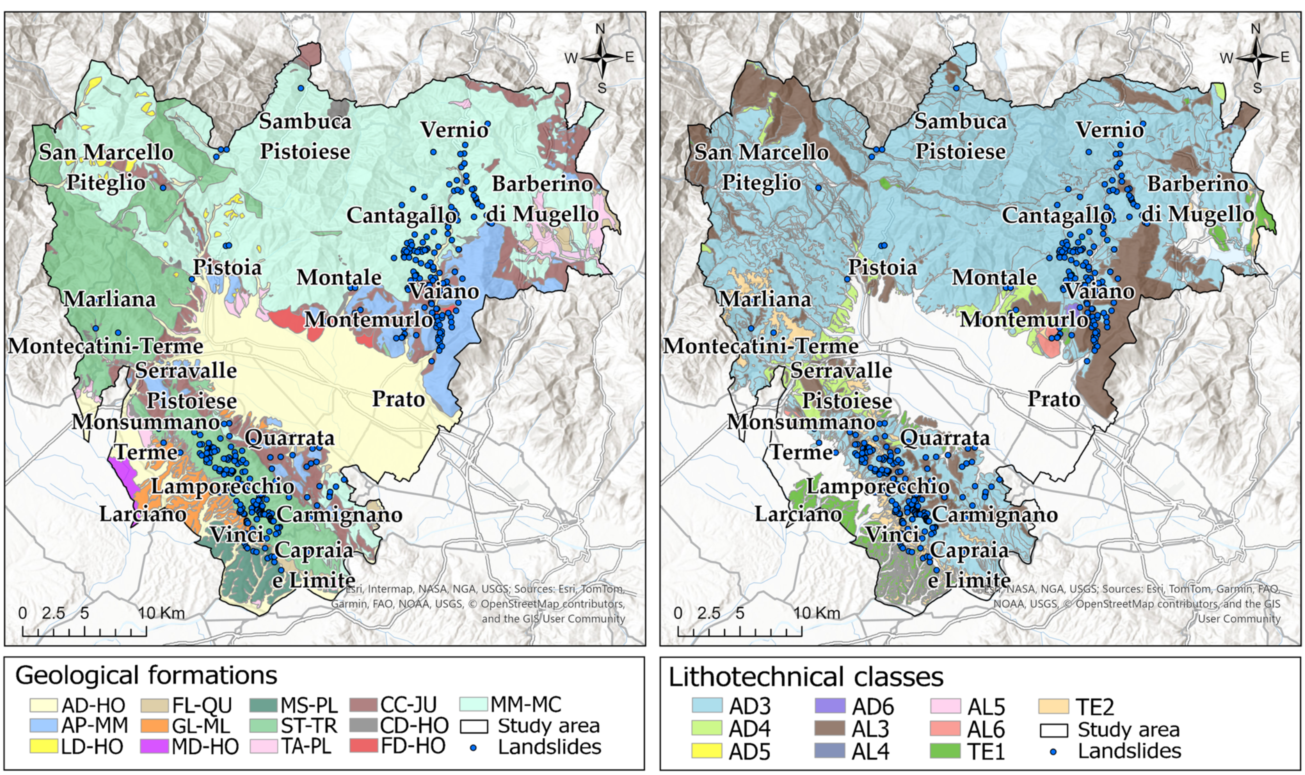

Fig. 2 Geological formations and lithotechnical classification of the study area (classes description in Tables 1 and 2)

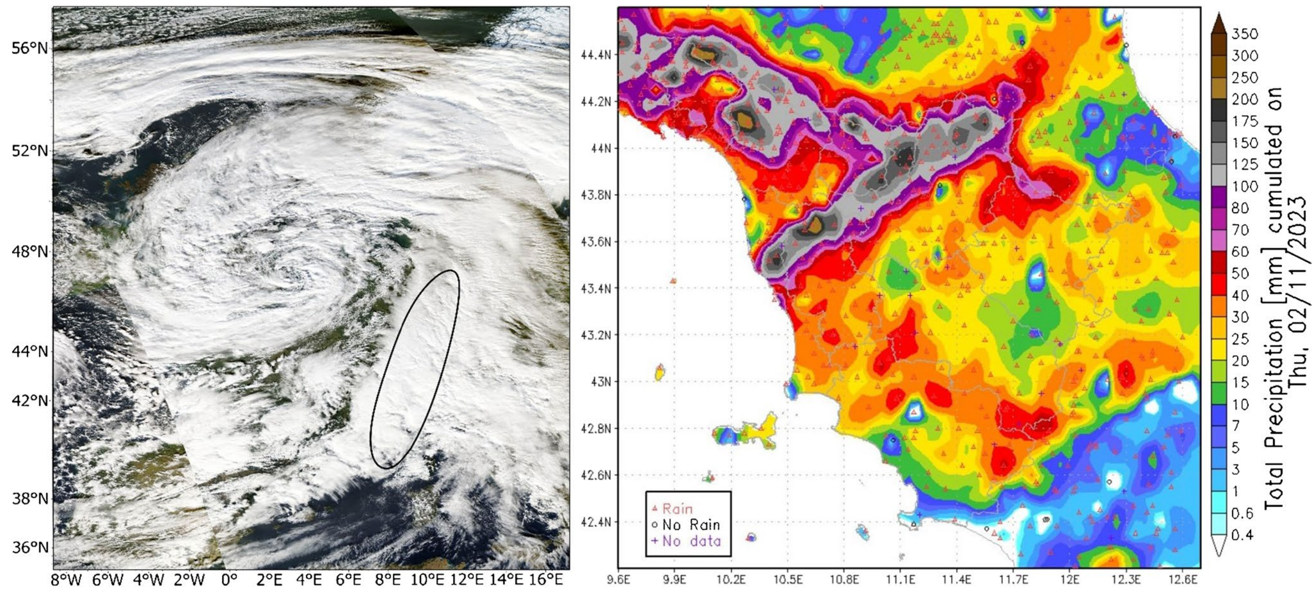

Fig. 3 "2 November 2023" meteorological event: **a** Satellite image of the approaching storm (position of the cold front highlighted in black) to the Tuscany region during the morning of 2 November (modified from https://worldview.earthdata.nasa.gov/); **b** 24 h cumulative rainfall recorded by rain gauges in central Italy (modified from "Report meteorologico Evento 2 novembre 2023")

part of the region with south–southwesterly winds advecting from the Ligurian Sea, combined with the simultaneous inflow of moderately cooler air at higher altitudes. The location, intensity, and especially the stationarity of this thunderstorm system turned out to be difficult—if not impossible—to predict (Bartolini et al. 2023; Report meteorologico Evento 2023).

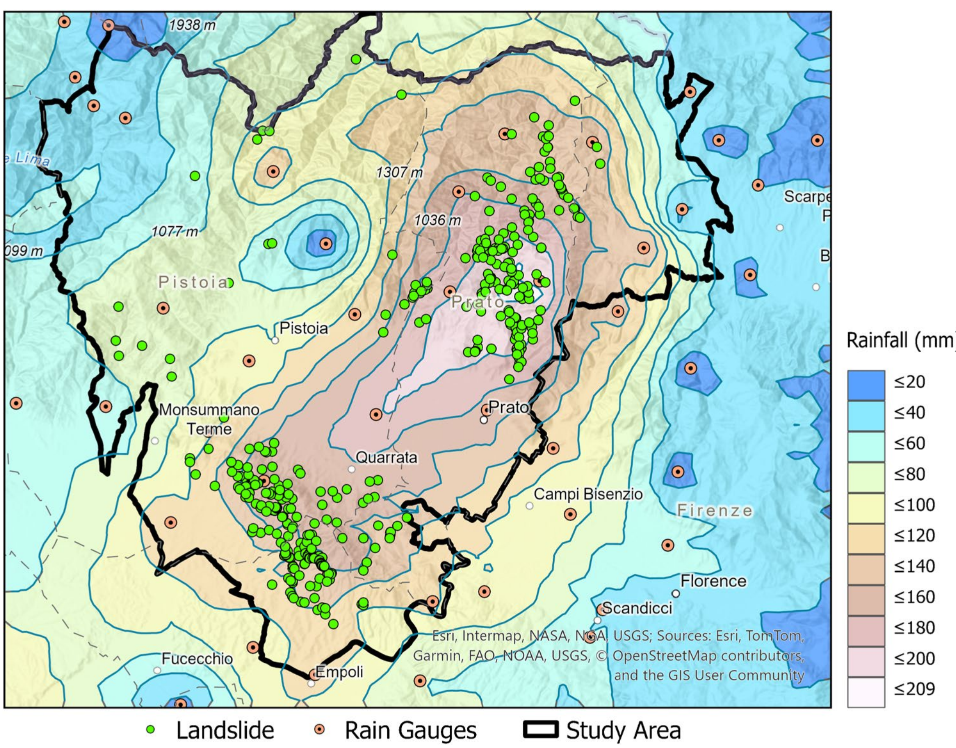

Fig. 4 Distribution of landslides and 24 h cumulative rainfall (mm) of the study area from radar and rain gauges data

Table 1 Geological formations of the study area

Code	Geological formation	Age	Description
MM-MC	Monte Modino – Monte Cervarola Unit	Late Cretaceous to Eocene	Turbiditic flysch of arenaceous-pelitic composition; part of the External Ligurian Units, deformed during Apennine orogenesis
AD-HO	Recent and active alluvial deposits	Holocene	Unconsolidated sand, silt, and gravel in active riverbeds and floodplains
ST-TR	Tuscan stratigraphic complex	Triassic to Early Miocene	A tectonostratigraphic unit composed of sedimentary successions including dolostones, marls, and limestones
CC-JU	Canetolo Complex	Jurassic to Late Cretaceous (emplaced in Eocene)	Chaotic mélange with limestone, basalt, radiolarite blocks in clayey matrix; formed in an accretionary wedge setting
AP-MM	Alberese/Pietraforte Group – Monte Morello Unit	Upper Jurassic to Eocene	Sedimentary succession including micritic limestone (Alberese) and massive sandstone (Pietraforte)
GL-ML	Lacustrine and fluvio-lacustrine deposits (Garfagnana, Lucca–Montecarlo–Lamporecchio)	Middle to Late Pleistocene	Fine-grained continental sediments in tectonic basins and paleo-lakes
TA-PL	Terraced alluvial deposits	Late Pleistocene	River terrace deposits shaped by glacial-interglacial incision phases
MS-PL	Lower to Middle Pliocene marine succession	Early to Middle Pliocene	Marine succession composed of clay, silt, and fine sand, often fossiliferous, deposited in shallow marine environments
FL-QU	Lacustrine and fluvio-lacustrine deposits (Florence–Pistoia–Prato)	Middle to Late Pleistocene	Fluvio-lacustrine deposits in the Florence–Pistoia–Prato area, typically silty-clayey, formed in tectonic basins
FD-HO	Fan deposits	Holocene	Poorly sorted gravel and sandy debris-flow deposits at the base of slopes
CD-HO	Colluvial deposits	Late Pleistocene to Holocene	Slope debris from weathering and gravity-driven processes, generally unstratified and heterogeneous
LD-HO	Landslide deposits	Late Pleistocene to Holocene	Deposits from mass movements (slides, flows, falls)
MD-HO	Marsh deposits	Holocene	Organic-rich clays and silts accumulated in low-energy wetland environments

Until 4:00 PM, precipitation mainly affected the northwestern areas (the hills of the provinces of Massa-Carrara, Lucca, and Pistoia), with localized maximum accumulations of up to 90–110 mm. Subsequently, the nearly stationary thunderstorm line recorded localized maximum accumulations of up to 180–200 mm in 3 h in the northern areas of the provinces of Pisa and Livorno, and up to 130–170 mm in 5–6 h in the southern areas of the province of Pistoia, the Montalbano area, and the province of Prato. During the 24 h of 2 November, more than 200 mm of rainfall had been recorded locally in the Apennine area of the province of Massa-Carrara, between the Apuan Alps and Garfagnana. Rainfall totals of 150–200 mm were also reached in the flood-affected areas of the provinces of Prato and Pistoia. Hourly rainfall intensities reached 80–100 mm between the provinces of Livorno and Pisa, and 40–55 mm between the provinces of Pistoia and Prato. The return periods for the precipitation event were estimated to be up to 150–200 years (Bartolini et al. 2023; Consorzio LaMMA 2023).

Figure 4 shows the distribution of landslides that occurred during the 2 November event across a 24 h cumulative rainfall (mm) map of the study area. The map of cumulative rainfall was obtained from radar images of the precipitable water content rectified using precipitation data from rainfall gauges present in the area (more details in section "Materials").

Table 2 Lithotechnical classification of the study area

Lithotechnical class	Description
AD3	Weak to very weak rock masses with persistent and regular discontinuities
AD4	Weak to very weak rock masses with persistent irregular discontinuities
AD5	Weak to very weak rock masses without discontinuities consisting of heterometric components
AD6	Weak to very weak rock masses without discontinuities with massive or equigranular texture
AL3	Medium to good-quality lithified rock masses with persistent and regular discontinuities
AL6	Medium to good-quality lithified rock masses with persistent and regular discontinuities
TE1	Fine grained soils
TE2	Medium- to coarse-grained soils
NC	Not classified (highly urbanized soils)

Methods

The approach adopted for the identification and mapping of landslides is based on i) image segmentation, ii) use of the Normalized Difference Vegetation Index (NDVI), iii) interpretation of pre- and post-event optical imagery, and iv) field surveys.

Image segmentation enables transforming pixel-based data into spatially and spectrally coherent objects, facilitating more effective feature extraction and classification in Geographic Information Systems (GIS) (Tavakkoli Piralilou et al. 2019). In this study, segmentation was conducted using the Mean Shift algorithm (Tao et al. 2007), which clusters pixels based on spectral and spatial similarity. NDVI index was used for detecting vegetation disturbances caused by landslides (Mondini et al. 2011; Gomes et al. 2020).

The core of the landslide identification was represented by a geomorphological interpretation in a GIS environment, integrating high-resolution pre- and post-event optical imagery with a 10-m resolution Digital Elevation Model (DEM) for a three-dimensional representation of the terrain and using supporting information from the image segmentation and the NDVI application.

In addition to remotely sensed data, the inventory incorporates a set of point-based landslide reports provided by the Regional Administration within the framework of the SOUP database. These points derive from official notifications submitted by local authorities (e.g., municipalities, civil protection units, local surveyors) in the immediate aftermath of the rainfall event and mainly refer to small-scale slope failures affecting roads, embankments, and minor channels. However, some of these reports could not be reported as polygons since they were not clearly recognizable on the available post-event satellite imagery. This was mostly due to: (i) the small size of the failures, often below the effective spatial resolution of the imagery; (ii) rapid removal of mobilized material during emergency and maintenance interventions; and (iii) the time lag between the event occurrence (2 November 2023) and the first suitable cloud-free satellite acquisitions, exceeding 20 days in some sectors. Nonetheless, such a database is a valuable source of information that better characterizes the impact of the rainfall event on the territory. Field surveys were conducted in the months following the rainfall event to validate preexistent point-based event databases, perform a visual recognition of the landslides remotely identified, and detect potential unrecognized phenomena. The initial phase of field surveys focused on the lower Bisenzio valley (in the localities of Schignano, Migliana, and Carmignanello) within the municipalities of Vaiano and Cantagallo. A second phase was carried out in the upper Val di Bisenzio, covering areas within the municipality of Vernio and adjacent territories such as the western sector of Barberino di Mugello and the mountainous areas of Montemurlo. Further surveys were then conducted along the Montalbano ridge, initially in the northern-facing slopes (municipalities of Quarrata and Carmignano) and subsequently in the southern sector (municipalities of Vinci, Lamporecchio, and Larciano).

The spatial distribution of landslides was analyzed to examine their occurrence in relation to rainfall conditions and predisposing factors by computing landslide frequency distributions across different factor classes, and by complementing this analysis with an exploratory multivariate approach.

Materials

Two optical multispectral satellite datasets were acquired, consisting of 4 PlanetScope images and 33 GeoEye-1 images, acquired on November 25 and 23, 2023, respectively. As pre-event reference data, satellite imagery from Google Earth and the ESRI basemap was used, dating back to May–June 2023 and March 2023, respectively.

These pre- and post-event images were the closest in time to the event among those meeting the requirements for detecting small landslides. Given the time interval between image acquisition and the November 2 event, it is possible that landslides caused by separate rainfall events were not distinguished. The temporal gap was, however, not considered critical, as no widespread triggering precipitation occurred during those periods, except on 2 November. To address the possibility that localized rainfall events may have triggered shallow landslides outside the main event window, relevant regional reports, landslide databases, and news sources were consulted. Even if a few minor landslides occurred during those isolated events and went unreported, their influence on the final inventory and related statistics is considered reasonably negligible.

Table 3 Land cover classification of the study area

Class	Description
3114	Forests dominated by chestnut
3115	Forests dominated by beech
2111	Intensive arable crops
223	Olive groves
3131	Mixed forests dominated by broad-leaved trees
242	Complex cultivation patterns
112	Discontinuous urban fabric
3132	Mixed forests dominated by conifers
3112	Forests dominated by deciduous oak species
3113	Mixed forests dominated by mesophilous and mesothermic broad-leaved trees
243	Land principally occupied by agriculture, with significant areas of natural vegetation
221	Vineyards
121	Industrial or commercial units
3117	Broad-leaved forests and plantations dominated by non-native species
3122	Forests dominated by mountain and oromediterranean pines
231	Herbaceous cover: perennial grasses not subject to crop rotation
324	Transitional woodland-shrub
3211	Alpine pastures (buildings and annexes)
334	Burnt areas
3121	Forests dominated by Mediterranean pines and cypress woods
512	Water bodies
111	Continuous urban fabric
142	Sport and leisure facilities
2112	Extensive arable crops
3123	Forests dominated by silver fir and/or Norway spruce
133	Construction sites
3212	Alpine pastures
122	Road and rail networks and associated land
141	Green urban areas
411	Inland marshes
3125	Coniferous forests and plantations dominated by non-native species
511	Watercourses
222	Fruit trees and berry plantations
333	Sparsely vegetated areas
131	Mineral extraction sites

Table 4 Dataset utilized for cn of the landslide inventory and assessment of landslides distribution as a function of environmental conditioning factors (details and sources in "Materials" section)

Landslides detection	Optical imagery from Planet Scope satellite Optical imagery from GeoEye-1 satellite
	Google Earth imagery
	ESRI imagery
	Italian Landslide Inventory (IFFI)
	Operational Document for Soil Protection (DODS)
	Surveys portal
	System of the Unified Civil Protection Operations Room (Civil Protection – SOUP RT)
Environmental conditioning factors analysis	Geological Formations Lithotechnical classification
	Corine Land Cover (CLC)
	Tinitaly 10 m DEM (elevation, slope angle and curvature)
	Soil Database (hydraulic conductivity and clay content)
	Rain gauges network
	National Radar Platform

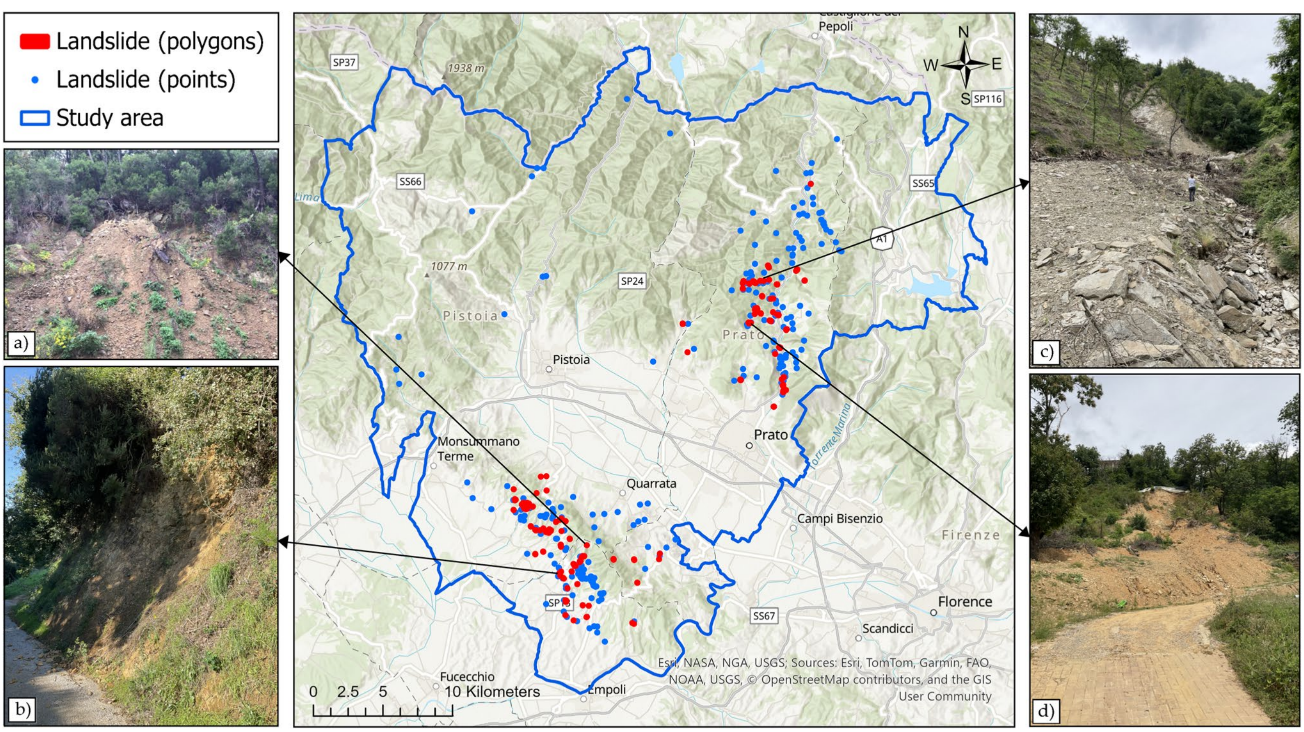

Fig. 5 Landslides distribution. (**a**, **b**) Landslides in Vinci municipality (197.7 m^2 and 23.5 m^2, respectively). (**c**) Landslide in Cantagallo municipality (3542.4 m^2). (**d**) Landslide in Vaiano municipality (1393.47 m^2)

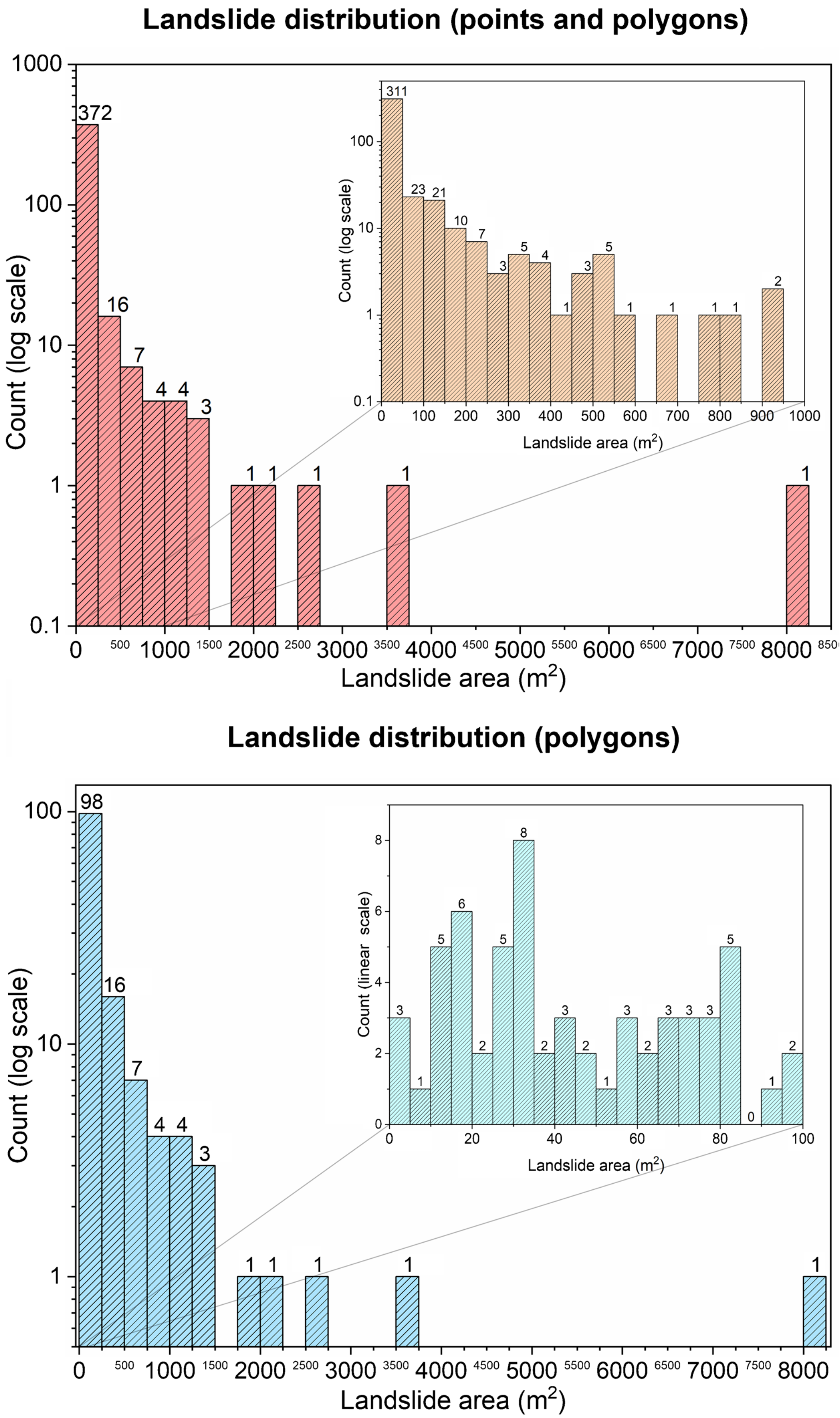

Fig. 6 Landslide distribution according to the areal extent. Top: landslide distribution—points and polygons, inset range 0–1000 m^2. Bottom: landslide distribution—only polygons, inset range 0–100 m^2

Table 5 Buildings impacted by landslides (polygons with 50-m buffer). Area refers to the total surface of building class intersecting the mapped landslide polygons, including the surrounding 50-m buffer

Building class	Number of elements	Area (square meters)
Residential	49	22,900
Agricultural	19	403
Power station	1	555
Place of worship	1	171
Social care facility	1	291
Industrial	6	4351
Other	60	7426

Table 6 Roads impacted by landslides (polygons with 50-m buffer). Length refers to the total length of road class intersecting the mapped landslide polygons, including the surrounding 50-m buffer

Road class	Number of elements	Length (meters)
Municipal roads	95	17,857.44
Provincial roads	19	2833.735
Private roads	6	469.029
Regional roads	4	450.124

PlanetScope consists of multiple CubeSat (known as Doves and Super Doves) launches in sun-synchronous orbit, offering up to 3 m multispectral imagery with daily revisit. Dove satellites (Standard PlanetScope) are the earlier-generation satellites, collecting 4-band multispectral imagery (Blue, Green, Red, and Near Infrared). SuperDoves (upgraded PlanetScope satellites) have been launched since 2020 and collect 8-band multispectral imagery with narrower and calibrated bands in the wavelength range of 430–860 nm. GeoEye-1 is an Earth observation satellite launched on September 6, 2008, part of the WorldView constellation, capable of revisiting any point on Earth every three days collecting imagery in 0.41 m panchromatic and 1.65 m four-band multispectral modes. Using the images from PlanetScope and GeoEye-1, two different mosaics (one for each dataset) were generated, both covering the entire study area.

As supporting sources of information for the identification and mapping of the shallow landslides triggered during the rainfall event, open sources data from national and regional administrations, along with non-public data provided directly from the Region were used.

Open data from (i) Inventario dei Fenomeni Franosi in Italia (Italian Landlside Inventory, IFFI), a standardized geospatial catalog of landslide events across Italy (https://idrogeo.isprambiente.it/app/); (ii) *Documento Operativo per la Difesa del Suolo* (Operational Document for Soil Protection, DODS), approved annually by the Regional Council, establishes the scope, timing, and funding of interventions including hydraulic infrastructure, slope stabilization, and maintenance works—https://geoportale.lamma.rete.toscana.it/difesa_suolo/#/viewer/769).

Non-publicly accessible data instead from i) Surveys portal, a platform collecting data from all field surveys carried out on landslides; ii) Civil Protection – SOUP RT (System of the Unified Civil Protection Operations Room of the Tuscany Region), a web-based application that gathers all reports of critical events occurring across the regional territory.

Rainfall data of the triggering event from different sources were collected. Rain gauge data were obtained from the regional rain gauge network managed by the Centro Funzionale della Regione Toscana (CFR—https://www.sir.toscana.it/consistenza-rete). This network comprises a distributed system of automated meteorological stations that continuously monitor precipitation (along with other hydrometeorological parameters) across the Tuscany region. For the present study, rainfall time series from 46 selected stations located within or near the study area were extracted and processed (Fig. 3). In addition to these, radar-derived rainfall data were obtained from the National Radar Platform (Piattaforma Nazionale Radar—https://mappe.protezionecivile.gov.it/it/mappe-rischi/piattaforma-radar), coordinated by the Italian Civil Protection Department. The platform provides open access (among other radar-derived data) to the Surface Rainfall Intensity (SRI): spatially continuous precipitation data (spatial resolution of 1 km^2) representing an estimate of surface rainfall intensity (expressed in mm/h) based on the combination of data from the national weather radar network and rain gauge stations. The radar data used in this study were retrieved from the archived dataset and processed to extract cumulative rainfall values over the area of interest.

To explore the spatial relationship between the occurrence of landslides and different environmental factors, maps of the following parameters were used: geology, lithology, land cover, slope angle, elevation, profile curvature, hydraulic conductivity, soil clay content, friction angle, and cohesion.

Distribution of geological formations and lithological classes in the study area (Fig. 2) were obtained from a publicly available database provided by the Tuscany Region (https://www.regione.toscana.it/-/geoscopio). Classes and descriptions are presented in Tables 1 and 2. The database consulted for lithology of the area classifies outcropping formations and soils based on a geotechnical characterization carried out by means of extensive field measurements, surveys, and laboratory tests (scale of 1:10.000). For the objectives of this study, the original lithotechnical classes are further reclassified according to their strength, layering, and texture.

Land cover data were obtained from the CORINE Land Cover (CLC) 2018 dataset at Level IV (https://groupware.sinanet.isprambiente.it/uso-copertura-e-consumo-di-suolo/library/copertura-del-suolo/corine-land-cover/corine-land-cover-2018-iv-livello), developed by the European Environment Agency (EEA). The dataset used (a hierarchically structured classification of land use and land cover with a spatial resolution of 100 m) has Level IV representing an additional thematic refinement based on national elaborations by ISPRA (Istituto Superiore per la Protezione e la

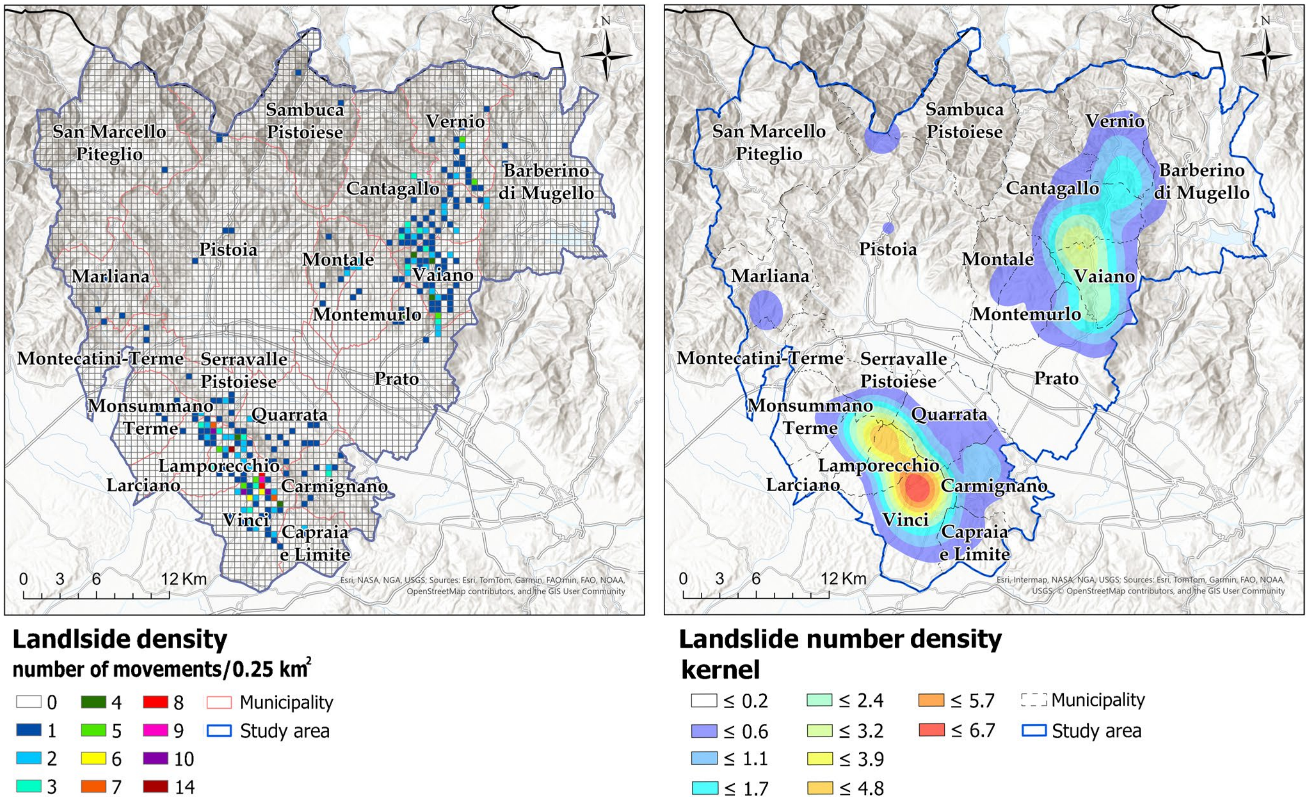

7 Landslide density and Kernel density maps

Ricerca Ambientale). CLC classes of the study area are presented in Table 3 (in order of areal extension).

Elevation, slope angle, and curvature were derived from a 10 m Digital Elevation Model (DEM) part of Tinitaly, a DEM of the Italian territory developed by the Istituto Nazionale di Geofisica e Vulcanologia (INGV) based on a Triangular Irregular Network (TIN) interpolation of elevation data from topographic maps and LiDAR acquisitions (https://tinitaly.pi.ingv.it).

Hydraulic conductivity and soil clay content were obtained from the 1:10,000 Scale Soil Database (Level 2–3) of the Tuscany Region, a detailed pedological dataset developed for land management, environmental planning, and agroforestry applications providing region-wide soil information based on systematic field surveys and analyses (https://www.regione.toscana.it/pedologia). A summary of all datasets used in this study are presented in Table 4.

Results

A total of 411 landslides triggered during the 2 November event were identified and validated within the area analyzed. The mass movements are recognized as rapid shallow landslides and are mainly distributed in the Bisenzio Valley (northeastern portion of the study area) and in the Montalbano ridge area (southwestern portion) (Fig. 5). The areal extension of the instabilities resulted limited, having approximately the 83% of the total an extension within 500 m^2 (Fig. 6). The 33% of the total (137 landslides) had an extension larger than 4.5 m^2 and was mapped as polygons, as their boundaries could be accurately delineated by means of the geomorphological interpretation on the satellite images validated then at the survey scale (Fig. 5). The remaining 274 landslides, smaller than 4.5 m^2, were represented as points placed approximately at their center (Fig. 5). This choice has been taken to avoid inaccuracy in their mapping, their limited size indeed—making them unrecognizable on satellite imagery—and simultaneously in many cases, their inaccessibility in the field (steep slopes, private lands, barriers for safety), prevented accurate boundary mapping. Some of them could be anyway mapped by means of field activity, but without the support of satellite images, a non-feasible (considering number and distribution of the landslides) survey activity should be carried out to avoid geometrical distortions.

The 137 landslides mapped as polygons cover a total area of 48,265 m^2, with an average extension of 352 m^2, ranging from a minimum of 4.5 m^2 to a maximum of 8,020 m^2. Considering that the landslides mapped as points had a minimum extension of approximately 3 m^2 (this was taken as the minimum threshold to classify a movement of mass as a landslide in this study, since for smaller extensions it is difficult to discriminate whether the kinematic—downstream displacement by gravity—and mechanical—breakage or deformation of the material—criteria were met) and a maximum of 4.5 m^2, their average extension can be estimated at approximately 3.7 m^2, so that the estimated total area affected by landslides reaches 49,292 m^2.

A 50-m buffer around landslides mapped as polygons was used to assess the influence of such events on buildings and infrastructures (Tables 5 and 6). The buffer around the mapped landslide polygons was not introduced to address spatial uncertainty

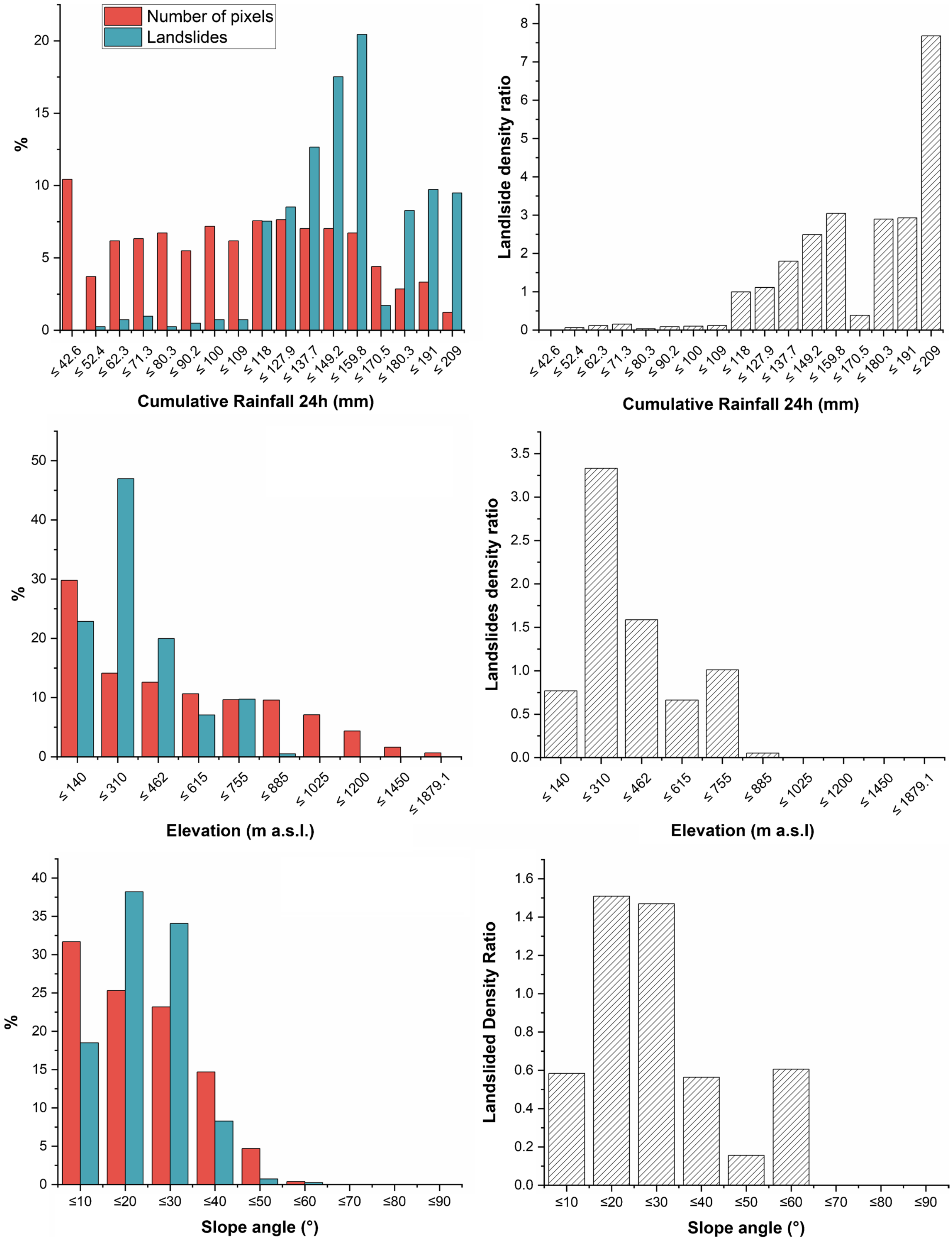

Fig. 8 Distributions of landslides across different classes of influencing variables (24 h cumulative rainfall, elevation, and slope angle). Left panel: Blue bars represent the percentage of landslides in each class; red bars indicate the percentage of the study area (i.e., number of pixels) falling within the classes. Right panel: landslide density ratio (ratio between the percentage of landslides occurring within a given class and the percentage of the study area covered by that class)

in landslide location, as landslides were field-mapped and their boundaries are known with sufficient accuracy. Rather, the buffer was used to represent the zone of influence of landslide impacts, which may extend beyond the area directly affected by landslide material. Although some landslides did not physically intersect buildings or roads, their close proximity resulted in indirect impacts and functional disruption. These included temporary loss of accessibility or usability due to safety inspections of buildings and roads, precautionary closures, traffic interruptions, and the installation of emergency or stabilization measures. Consequently, buildings and infrastructure located within the buffer cannot be regarded as unaffected, even in the absence of direct physical damage. The buffer therefore captures real, observed consequences of landslide occurrence, rather than hypothetical effects or modeling uncertainty.

A total of 120 buildings were affected, the vast majority of which are classified as "other" (e.g., agricultural sheds or ancillary buildings in rural areas), totaling 61 structures, followed by 49 residential buildings. In total, approximately 21,600 m of roads were affected. Affected buildings and roads are defined here as those spatially intersecting the mapped landslide polygons or their surrounding 50-m buffer, which was adopted to account for indirect impacts and functional disruption. This spatial-based assessment provides an objective and reproducible indication of the overall magnitude of landslide impacts.

The majority of the impacted roads correspond to municipal roads, with 95 segments impacted, totaling about 17,857 m. This was followed by provincial roads (19 segments, 2,833 m), private roads (6 segments, 469 m), and a limited number of regional roads (4 segments; 450.124 m). These results highlight a stronger impact on the secondary road network, particularly local infrastructure. Landslides affecting these roads often led to the isolation of peripheral settlements, as such infrastructures frequently constitute the sole access to small villages. This has caused significant disruptions in mobility and in the delivery of essential services. In many cases, restoration interventions were delayed or prolonged due to the complexity of the terrain and limited availability of alternative routes. These conditions have contributed to an increase in indirect economic losses, which are difficult to quantify, and led to a substantial deterioration in the quality of life for the affected local population.

Spatial distribution of landslides was investigated by means of i) a raw landslide density to obtain actual values of event concentration across the study area and ii) a kernel density estimation to better capture spatial clustering and to highlight the main trends and patterns of landslide occurrence.

The highest landslide densities (expressed as number of mass movements per 0.25 square meters of area) resulted in the Montalbano ridge area (southwestern part of the study area), where densities of 12–14 landslides per 0.25 km^2 are reached. Medium densities were found in the Bisenzio valley where the landslide concentration peaks at 5 events per 0.25 km^2. The highest average densities per municipality resulted in 0.7, 0.6, and 0.5 average landslides per 0.25 km^2 (Lamporecchio, Vinci, and Vaiano municipalities respectively).

To investigate spatial clustering of landslides, a Gaussian kernel density estimation was carried out using a 1000-m search radius (Fig. 7). The resulting landslide number density (LND) map provides a continuous estimate of landslide concentration, expressed as events per square kilometer, allowing the identification of high-density zones and spatial patterns of occurrence. Two distinct clusters of high landslide density clearly emerge: the first and most prominent is located in the central-southern sector, where density values exceed 6 events/km^2; the second cluster, located in the north-eastern sector, exhibits a comparatively lower density but still reveals a significant aggregation of events.

Analysis of landslide occurrence in relation to rainfall conditions and predisposing factors

The relationship between landslide occurrence and a set of environmental predisposing and triggering factors was first assessed through a bivariate statistical approach, based on the spatial correlation between the distribution of mapped landslides and selected variables (Figs. 8, 9, and 10). These include daily cumulative rainfall on 2 November (triggering factor) and a set of morphometric, hydrological, geological, and land use parameters (elevation, slope, profile curvature, hydraulic conductivity, clay content, lithotechnical class, geological formations, and Corine Land Cover). For each variable, the study area was divided into discrete classes, and a Landslide Density Ratio (LDR) was calculated to assess the relative frequency of landslides in each class with respect to its areal extent (ratio between the percentage of landslides occurring within a given class and the percentage of the study area covered by that class). This approach allows identifying thresholds or ranges of values where landslide incidence is significantly higher than expected, thus highlighting the main conditioning and triggering factors during the event.

As relating to daily cumulative precipitation on 2 November (Fig. 8), a marked increase in landslide occurrence is observed beyond 109 mm of cumulative rainfall in 24 h, with LDRs values higher than ~ 2 for rainfall beyond 127.9 mm and reaching ~ 8 beyond 191 mm. While the causal relationship between intense precipitation and the triggering of shallow landslides was expected and widely documented in the literature, the aim of this analysis was to verify whether a precipitation threshold could be identified beyond which landslide occurrence significantly increases.

Landslides resulted occurring most frequently in the 140–310 m a.s.l. range, where a very high LDR (> 3.0) is observed. Both lower (≤ 140 m) and higher elevations (> 615 m) show LDR below 1, indicating reduced incidence relative to area (Fig. 8).

With respect to slope angle, instabilities are most common between 10° and 30°, where LDR peaks at around 1.5. Flatter slopes (≤ 10°) and steeper ones (> 40°) show reduced occurrence (LDR < 1), with the lowest value (0.24) observed in the 40°–50° class (Fig. 8).

The highest LDR (~ 2.6) is associated with concave profile curvatures (≤ −0.02). Slightly concave to planar surfaces (−0.007 to 0.012) show moderate values (~ 1), while convex areas (≥ 0.023) correspond to lower incidence (LDR < 0.5) (Fig. 9).

Instabilities are most frequent in zones with moderate hydraulic conductivity (1.14–2.11 m/day), where LDR reaches ~ 2. Elevated values are also seen for conductivity > 3.5 m/day. Conversely, lower LDRs occur between 2.1 and 3.5 m/day and below 0.4 m/day (Fig. 9). A clear trend associated with this parameter is not recognizable,

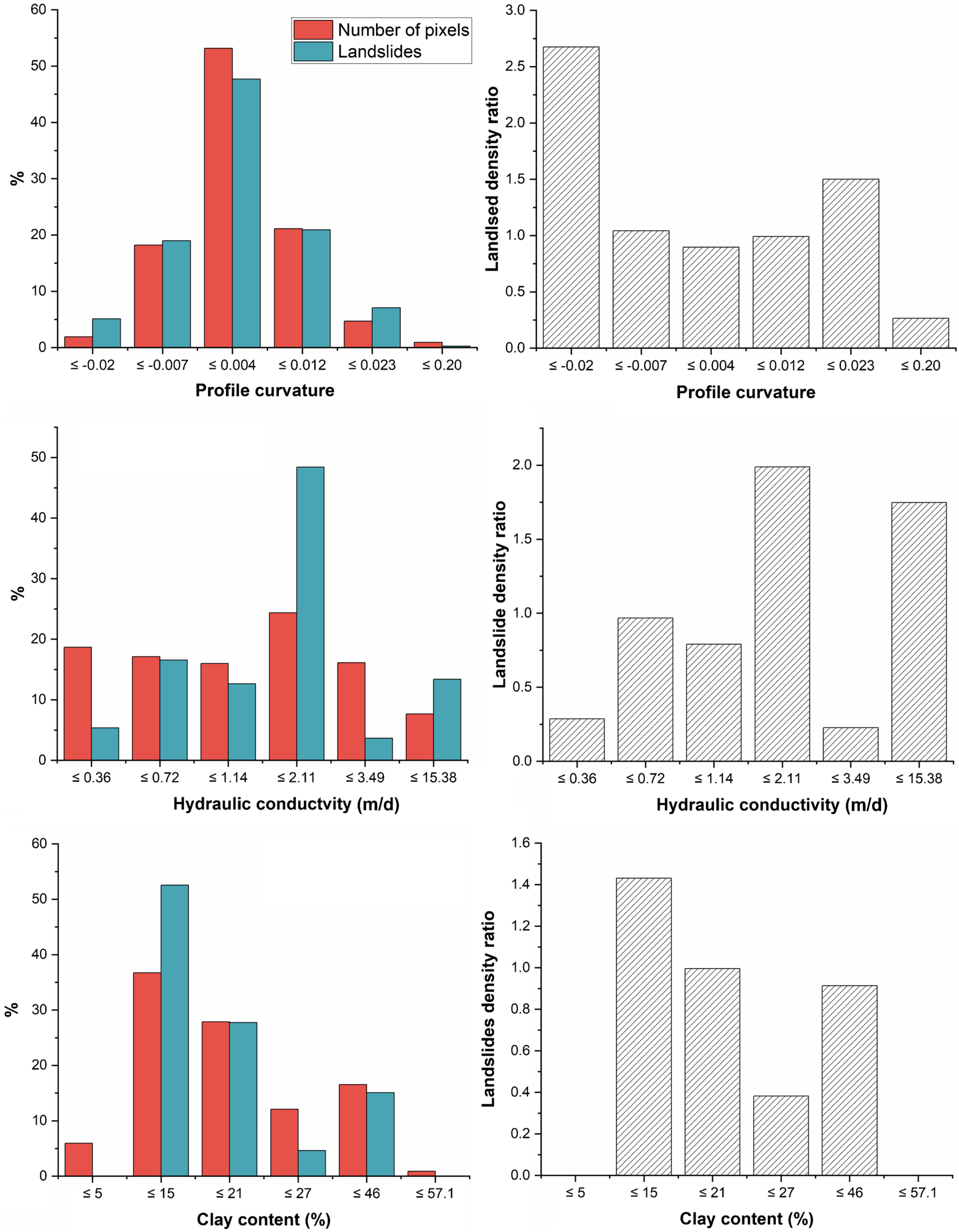
Number of pixels
Landslides
%
≤ -0.02
≤ -0.007
≤ 0.004
≤ 0.012
≤ 0.023
≤ 0.20
Profile curvature
Landlised density ratio
Profile curvature
%
≤ 0.36
≤ 0.72
≤ 1.14
≤ 2.11
≤ 3.49
≤ 15.38
Hydraulic conductvity (m/d)
Landslide density ratio
Hydraulic conductivity (m/d)
%
≤ 5
≤ 15
≤ 21
≤ 27
≤ 46
≤ 57.1
Clay content (%)
Landslides density ratio
Clay content (%)

◂**Fig. 9** Distributions of landslides across different classes of influencing variables (profile curvature, hydraulic conductivity, and clay content). Left panel: Blue bars represent the percentage of landslides in each class; red bars indicate the percentage of the study area (i.e., number of pixels) falling within the classes. Right panel: landslide density ratio (ratio between the percentage of landslides occurring within a given class and the percentage of the study area covered by that class)

suggesting that the combination with others is crucial for slope stability.

The highest LDRs are observed for the ST–TR (Tuscan stratigraphic complex) and GL–ML (Lacustrine and fluvio-lacustrine deposits) formations, both exhibiting LDR values around 2.5, indicating a landslide occurrence more than double their spatial representation (Fig. 10). The MS–PL (Lower to Middle Pliocene marine succession) formation also shows an elevated LDR of approximately 1.5, reflecting moderate susceptibility. Other formations with considerable spatial coverage, such as AP–MM (Alberese/Pietraforte Group – Monte Morello Unit) and CC–JU (Canetolo Complex), present LDR values close to 1, indicating a proportional landslide occurrence relative to their extent. MM–MC (Monte Modino – Monte Cervarola Unit) and AD–HO (Recent and active alluvial deposits) exhibit lower LDR values, suggesting a relatively lower propensity for landslides during the studied event.

Among lithotechnical units, the highest LDRs are observed in TE1 (Fine grained soils) and AL3 (Medium to good-quality lithified rock masses with persistent and regular discontinuities) with values higher than > 2.5 and equal to ~ 1.8, respectively. The most widespread unit (AD3, Weak to very weak rock masses with persistent and regular discontinuities) has an LDR close to 1, indicating proportional occurrence. The lowest values are recorded in TE2 (Medium- to coarse-grained soils), AD4 (Weak to very weak rock masses with persistent irregular discontinuities), and NC (Not classified—highly urbanized soils), likely reflecting a lower susceptibility (Fig. 10).

Finally, the highest LDR (> 4.5) is associated with CLC class 223 (Olive groves), followed by class 242 (Complex cultivation patterns) and 3131 (Mixed forests with a prevalence of broad-leaved trees), both with values close to 2. In contrast, extensive land cover types such as 2111 and 3115 (Intensive crops and beech forests) show very low values (< 0.1), together with 3114, 3112, and 3132 (chestnut- and oak-dominated woods, and coniferous forests), all below 0.6. Other classes with limited extent, such as mesophilous broad-leaved and Oromediterranean pine forests, also show minimal values (Fig. 10).

A principal component analysis (PCA) was then applied to the set of landslide conditioning factors (Fig. 11). Different configurations were tested, including the use of all available variables versus a reduced set of selected factors, and the inclusion of all landslide representations (points and polygons) versus mapped landslide polygons only.

When all variables and landslide representations (points and polygons) are considered, the first two principal components explain a limited proportion of the variance and no clear structure emerges. Conversely, restricting the analysis to selected variables (cumulative rainfall, clay content, land use, slope angle, and hydraulic conductivity), which exhibited clearer trends in the univariate analysis, and to mapped landslide polygons results in a clearer multivariate pattern. In this configuration, the first two principal components explain approximately 68% of the total variance (PC1 ≈ 41% and PC2 ≈ 27%). PC1 mainly reflects a gradient related to slope angle and soil hydraulic conductivity, opposed to clay content and rainfall-related variables, whereas PC2 is primarily associated with land-use characteristics. In all tested configurations, landslide data points are continuously distributed in the multivariate space, and no distinct clusters are observed.

Discussion

The compilation of the landslide inventory—based on the use of satellite imagery and field surveys—allowed for a detailed assessment of size and spatial distribution of the movements triggered during the November 2 rainfall event. The landslides that occurred during the event resulted predominantly from limited extension and were spatially concentrated (approximately 83% of the landslides exhibited an areal extent of less than 500 m^2, with a large proportion even smaller than 4.5 m^2). Such prevalence of small-scale movements, also observed in other extreme rainfall scenarios in recent years in Italy (Donnini et al. 2023; Santangelo et al. 2023; Confuorto et al. 2025; Berti et al. 2024), emphasizes the need for high-resolution remote sensing products combined with field validation to achieve a representative inventory.

Although most of the landslides involved limited volumes of ground material, their widespread spatial distribution resulted in a relevant cumulative impact on local infrastructure, particularly in rural and mountainous sectors. Over 21 km of roads were directly or indirectly affected, mostly municipal roads, which often represent the only access routes to scattered hamlets. In the present case, several of these roads remained interrupted for extended periods due to the complexity of the required restoration works. Most landslide events occurred in areas characterized by the absence of redundancy in the transport network, where only minor roads are present. As a result, access for emergency vehicles and maintenance machinery was locally difficult, slowing down response and recovery operations. In addition to temporary limitations to mobility and accessibility, these conditions also affected daily activities linked to agriculture and local economic practices, which are strongly dependent on road connectivity in these sectors.

The spatial distribution of landslides reveals distinct clustering patterns, with prominent concentrations localized in the Montalbano Ridge (southwestern sector) and Bisenzio Valley (northeastern sector). These spatial clusters do not exhibit a straightforward correlation with rainfall intensity patterns, highlighting the importance of a comprehensive analysis of the relationships between predisposing environmental factors and landslide occurrence to investigate the territory susceptibility to heavy rainfall, as similarly demonstrated in numerous studies (e.g., Guzzetti et al. 1999; Mondini et al. 2011).

However, the analysis of the spatial relationships between landslides distribution and rainfall intensity patterns allowed to preliminary identify a critical rainfall intensity threshold. The threshold identified—109 mm in 24 h—aligns with values reported in the scientific literature for landslide-prone regions in Italy and across Europe. In Italy, several studies of the last two decades have defined rainfall thresholds that ranging between 30 mm (in areas highly sensitive to slope instabilities) and 130 mm of cumulative rainfall in 24 h, depending mainly on local

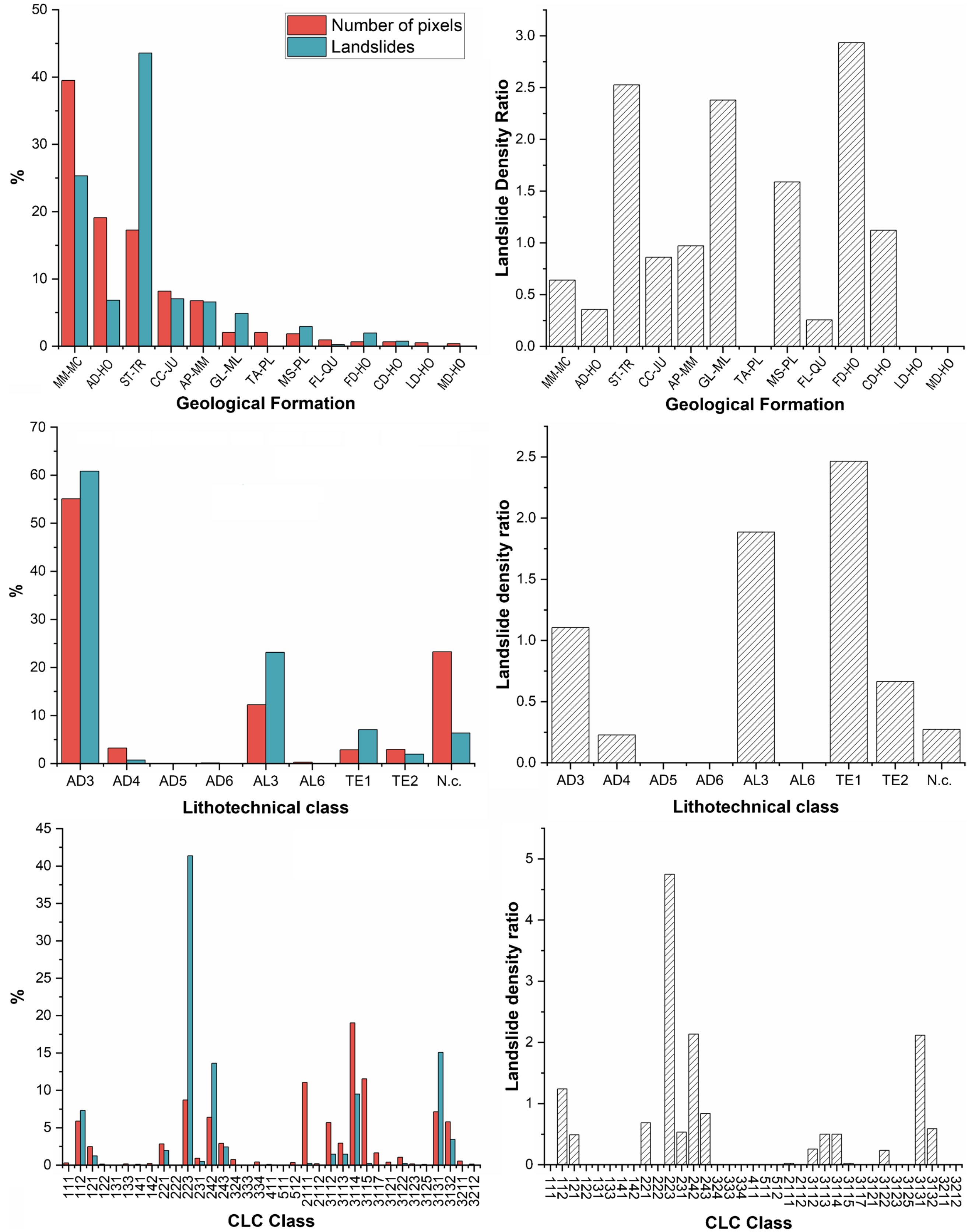

Number of pixels
Landslides
%
Landslide Density Ratio
Geological Formation
MM-MC
AD-HO
ST-TR
CC-JU
AP-MM
GL-ML
TA-PL
MS-PL
FL-QU
FD-HO
CD-HO
LD-HO
MD-HO
Landslide density ratio
Lithotechnical class
AD3
AD4
AD5
AD6
AL3
AL6
TE1
TE2
N.c.
CLC Class

◂**Fig. 10** Distributions of landslides across different classes of influencing variables (geological formations, lithotechnical classification, and land use; CORINE land cover, CLC, classes description in Tables 1, 2, and 3, respectively). Left panel: Blue bars represent the percentage of landslides in each class; red bars indicate the percentage of the study area (i.e., number of pixels) falling within the classes. Right panel: landslide density ratio (ratio between the percentage of landslides occurring within a given class and the percentage of the study area covered by that class)

lithology, slope morphology, and type of landslide (e.g. Guzzetti et al. 2008; Peruccacci et al. 2012; Brunetti et al. 2010; Gariano et al. 2015). The 109 mm/24 h threshold identified here falls within the medium-upper range of values commonly observed, suggesting that the slopes in the study area may exhibit relatively high resistance to initial triggering, yet become vulnerable under extreme rainfall events. Even if the identification of this threshold provides a contribution in understanding the hydrological conditions under which shallow landslides are triggered in the area, it is important to underline that this assessment should be considered only preliminary and the approach used simplified. Further dedicated investigations would be necessary, considering different triggering rainfall events, duration of rainfall and using appropriate statistical approaches.

The spatial distribution of landslides, analyzed in relation to the area's morphologic, hydrogeological, geotechnical, and land cover characteristics, facilitated the delineation of environmental conditions exhibiting heightened susceptibility to shallow landslide during the event. The highest LDR values are observed between 140 and 310 m a.s.l. and on slopes ranging from 10° to 30°. In contrast, steeper slopes (> 40°) show significantly lower landslide

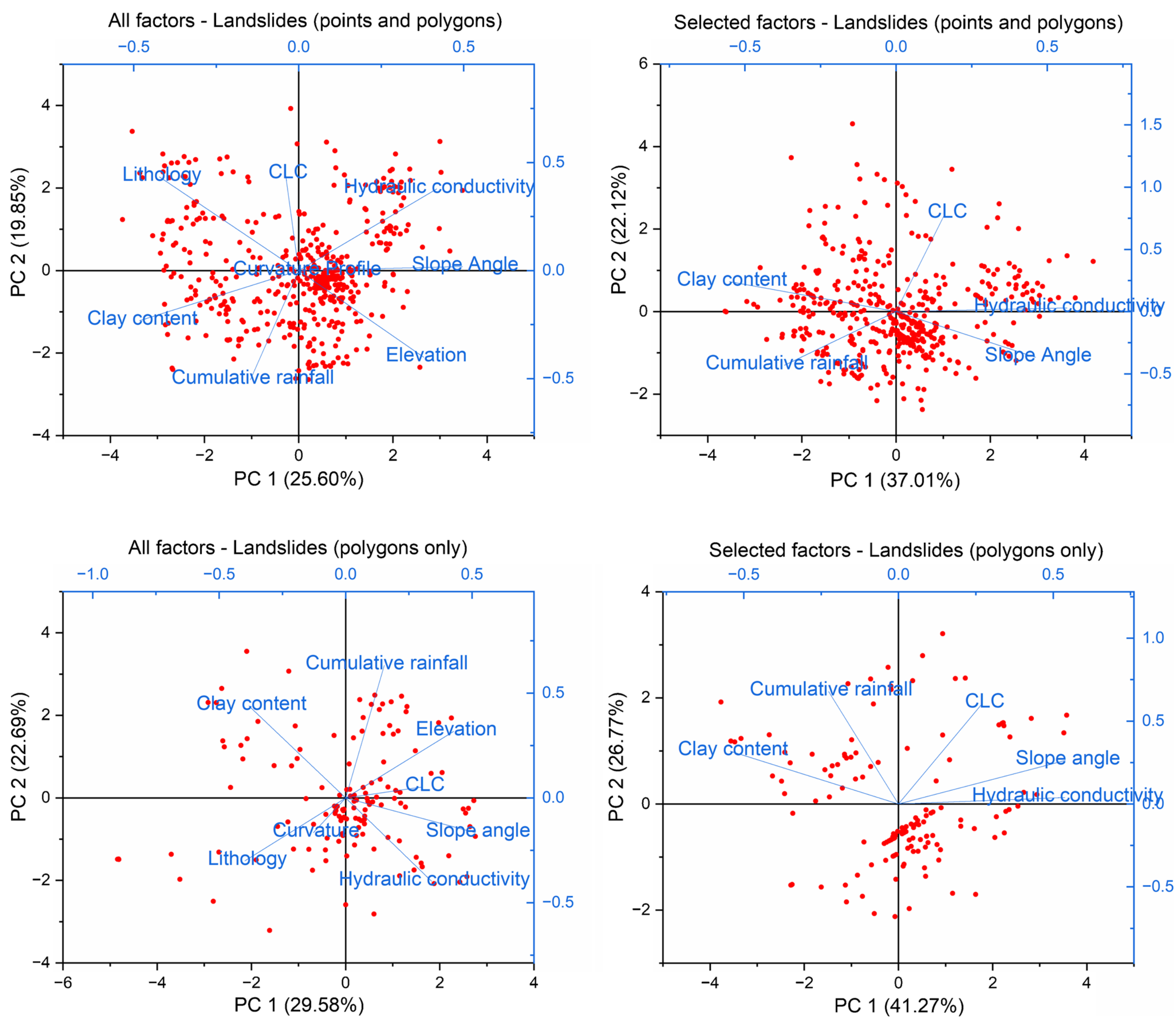

Fig. 11 PCA of conditioning factors: (top-left) all variables and all landslide representations; (top-right) selected variables and all landslide representations; (bottom-left) all variables and mapped landslide polygons only; (bottom-right) selected variables and mapped landslide polygons only

densities. This suggests that the greater gravitational potential of these slopes was effectively counteracted by their propensity to promote surface runoff during intense rainfall, limiting infiltration and consequently reducing the likelihood of pore-pressure build-up required for shallow landslide initiation. Landslide occurrence was more frequent in soils with intermediate hydraulic conductivity (1.14–2.11 m/day) and moderate clay content (5–15%), a combination (quite common in Tuscany, Masi et al. 2020; Vannocci et al. 2022) likely allowing substantial water intake without rapid drainage. This finding is further supported by the concentration of failures on moderately steep slopes, where infiltration remains effective while surface runoff is not yet dominant.

Interpreting the influence of geological formations on landslide susceptibility is challenging, as their spatial distribution is strongly linked to tectonic and geomorphological phenomena, so that the correlation with the slope gradient (and other factors dependent on the latter) can be high. The extended formation of ST-TR (Tuscan stratigraphic complex) showed a high LDR of 2.5, suggesting a higher landslide susceptibility. This unit, characterized by a tectonostratigraphic succession including dolostones, marls, and limestones, is often overlain by weathering-derived debris that reduces slope cohesion. But it is necessary to note that it largely corresponds to a prominent ridge (dorsal) in the study area.

The most affected lithotechnical units were AL3 and TE1. AL3 consists of lithified rock masses with medium to good geomechanical quality, characterized by persistent and regular discontinuities that may act as unstable support for overlying soils. TE1 is composed of fine-grained, weathered or colluvial materials, which represent shallow, easily saturable soils. The lateral coexistence and spatial interaction of these two contrasting materials may locally enhance the susceptibility to shallow translational landslides.

Regarding the highest LDR resulted associated with olive groves, it has to be considered that olive plantations are located on terraced or gently sloping hillsides. In addition to this, their rainfall interception and soil reinforcement—due to the mechanical action of the roots—capacities are low, both since they are typically sparse and that spontaneous vegetation is not allowed. These conditions contrast with dense natural forests, which provide both effective rainfall interception and root reinforcement, as reflected in the low LDR values for broad-leaved and coniferous woodland classes.

The analysis of landslide spatial distribution indicates that shallow failures predominantly occurred under environmental conditions characterized by intermediate slope angles, moderate infiltration capacity, and clay content, and land-use types associated with limited rainfall interception and weak root reinforcement.

The multivariate analysis indicates that landslide occurrence was not governed by a single dominant combination of conditioning factors. The absence of clearly separated clusters in the PCA suggests a diffuse landslide response to extreme rainfall forcing. In this context, the identified multivariate gradients should be interpreted as indicative of general predisposition patterns rather than deterministic controls. This behavior is consistent with the widespread spatial distribution of shallow landslides observed during the event and with the capacity of extreme rainfall to overcome local variability in predisposing conditions.

Conclusions

This study analyzed the shallow landslides triggered by the 2 November 2023 extreme rainfall event in Tuscany (central Italy), providing an event-based inventory and investigating the spatial distribution of failures in relation to triggering and predisposing factors. The inventory was constructed based on satellite images pre and post-event analyses and interpretation and was integrated/validated by means of extensive surveys.

Both univariate and multivariate analyses indicate that shallow landslides occurred preferentially under specific environmental conditions, without converging toward a single dominant combination of controlling factors.

The results allow to individuate a threshold of cumulated rainfall of ~ 109 mm/24 h as critical. The spatial pattern of failures reflects the interplay between geomorphological, pedological, lithological, and land use factors. The highest landslide densities were observed in areas characterized by intermediate slopes (10°–30°), moderate elevation (140–310 m a.s.l.), soils with intermediate hydraulic conductivity (1.14–2.11 m/day) and moderate clay content (5–15%). These conditions likely favored significant infiltration without rapid drainage, promoting pore-pressure build-up (top-down saturation) and shallow failure initiation. In terms of land cover, the highest landslides density ratio values were found in areas dominated by olive groves, likely due to their typically location on gentle or terraced slopes along with the limited vegetation cover, determining low root reinforcement and interception capacity—especially when compared to denser forested areas, which showed markedly lower landslide incidence.

The findings of this work underscore the relevance of detailed post-event inventories in identifying spatial patterns of landslide susceptibility. Moreover, the observed combinations of terrain, soil, geology, and land use contributing to failure initiation offer insights for improving forecasting systems, susceptibility modeling, emergency planning, and the design of adaptive land management strategies in the context of increasing climate-induced hydrogeological hazards.

Funding

Open access funding provided by Università degli Studi di Firenze within the CRUI-CARE Agreement. The research activity has been carried out in the framework of a research agreement between the Civil Protection Centre of the University of Florence and Regione Toscana.

Declarations

Competing interests The authors declare no competing interests.

References

Agnoletti C, Ferretti C, Ghezzi L, Maitino ML, Paniccià R, Patacchini V, Piccini L, Ravagli L, Sciclone N (2023) La quantificazione del danno da alluvione per imprese e famiglie. IRPET, Firenze. https://www.irpet.it/la-quantificazione-del-danno-da-alluvione-per-imprese-e-famiglie/. Accessed 3 Sept 2025

ANSA (2024) Alluvione in Toscana, censiti 2,7 miliardi di danni diretti. ANSA. https://www.ansa.it/toscana/notizie/2024/01/24/alluvione-in-toscana-censiti-27-miliardi-di-danni-diretti_93ad347d-14d6-46b4-a251-887233e87741.html . Accessed 3 Sept 2025

Bartolini C (2003) When did the northern Apennine become a mountain chain? Quat Int 101:75–80. https://doi.org/10.1016/S1040-6182(02)00090-3

Bartolini G, di Stefano V, Maracchi G, Orlandini S (2011) Mediterranean warming is especially due to summer season. Theor Appl Climatol 107(1):279–295. https://doi.org/10.1007/S00704-011-0481-1

Bartolini G, Grifoni D, Torrigiani T, Vallorani R, Meneguzzo F, Gozzini B (2014) Precipitation changes from two long-term hourly datasets in Tuscany, Italy. Int J Climatol. https://doi.org/10.1002/joc.3956

Bartolini G, Morabito M, Crisci A, Grifoni D, Torrigiani T, Petralli M, Maracchi G, Orlandini S (2008) Recent trends in Tuscany (Italy) summer temperature and indices of extremes. Int J Climatol 28:1751–1760. https://doi.org/10.1002/joc.1673

Bartolini G, Grasso V, Betti G, Fibbi L, Grifoni D, Messeri G, Tei C, Malaspina Torrigiani T, Vallorani R (2023) INVERNO 2023. Report meteo-climatico sulla Toscana. Zenodo. https://doi.org/10.5281/zenodo.7867821

Berti M, Pizziolo M, Scaroni M, Generali M, Critelli V, Mulas M, Tondo M, Lelli F, Fabbiani C, Ronchetti F, Ciccarese G, Dal Seno N, Ioriatti E, Rani R, Zuccarini A, Simonelli T, Corsini A (2025) RER2023: the landslide inventory dataset of the May 2023 Emilia-Romagna meteorological event. Earth Syst Sci Data 17(3):1055–1074. https://doi.org/10.5194/essd-17-1055-2025

Berti M, Pizziolo M, Scaroni M, Generali M, Critelli V, Mulas M, ... Corsini A (2024) RER2023: the landslide inventory dataset of the May 2023 Emilia-Romagna event. Earth System Science Data Discussions, 2024, 1-24. https://doi.org/10.5194/essd-17-1055-2025

Bortolotti V (1992) Guida geologica. Vol. 4: Appennino tosco-emiliano. Be-Ma, Milano

Brunetti MT, Peruccacci S, Rossi M, Luciani S, Valigi D, Guzzetti F (2010) Rainfall thresholds for the possible occurrence of landslides in Italy. Nat Hazards Earth Syst Sci 10(3):447–458. https://doi.org/10.5194/nhess-10-447-2010

Carmignani L, Kligfield R (1990) Crustal extension in the Northern Apennines: the transition from compression to extension in the Alpi Apuane core complex. Tectonics 9(6):1275–1303. https://doi.org/10.1029/TC009i006p01275

Catani F (2021) Landslide detection by deep learning of non-nadiral and crowdsourced optical images. Landslides 18(3):1025–1044. https://doi.org/10.1007/s10346-020-01513-4

Confuorto P, Franceschini R, Scarpitta L, Casagli N, Morelli S, Raspini F, Tofani V, Moretti S (2025) Event-based landslide inventory through very high-resolution optical images and field surveys. Geoenviron Disasters 12(1):23. https://doi.org/10.1186/s40677-025-00328-6

Consorzio LaMMA (2023) Laboratorio di Monitoraggio e Modellistica Ambientale - Report meteorologico Evento 2 novembre 2023, (https://www.lamma.toscana.it/clima/report/eventi/evento_02112023.pdf)

Davolio S, Della Fera S, Laviola S, Miglietta MM, Levizzani V (2020) Heavy precipitation over Italy from the Mediterranean storm "Vaia" in October 2018: assessing the role of an atmospheric river. Mon Weather Rev 148(9):3571–3588. https://doi.org/10.1175/MWR-D-20-0021.1

Del Soldato M, Riquelme A, Bianchini S, Tomás R, Di Martire D, De Vita P, Moretti S, Calcaterra D (2018) Multisource data integration to investigate one century of evolution for the Agnone landslide (Molise, southern Italy). Landslides 15(11):2113–2128. https://doi.org/10.1007/s10346-018-1015-z

Diakakis M, Mavroulis S, Filis C, Lozios S, Vassilakis E, Naoum G, Soukis K, Konsolaki A, Kotsi E, Theodorakatou D, Skourtsos E, Kranis H, Gogou M, Spyrou NI, Katsetsiadou K-N, Lekkas E (2023) Impacts of Medicanes on geomorphology and infrastructure in the eastern mediterranean, the case of Medicane ianos and the ionian islands in western Greece. Water 15(6):1026. https://doi.org/10.3390/w15061026

Dietrich A, Krautblatter M (2017) Evidence for enhanced debris-flow activity in the Northern Calcareous Alps since the 1980s (Plansee, Austria). Geomorphology 287:144–158. https://doi.org/10.1016/j.geomorph.2016.01.013

Donnini M, Santangelo M, Gariano SL, Bucci F, Peruccacci S, Alvioli M, Althuwaynee O, Ardizzone F, Bianchi C, Bornaetxea T, Brunetti MT, Cardinali M, Esposito G, Grita S, Marchesini I, Melillo M, Salvati P, Yazdani M, Fiorucci F (2023) Landslides triggered by an extraordinary rainfall event in Central Italy on September 15, 2022. Landslides 20(10):2199–2211. https://doi.org/10.1007/s10346-023-02109-4

Elter P, Giglia G, Tongiorgi M, Trevisan L (1975) Tensional and compressional areas in the recent (Tortonian to present) evolution of the northern Apennines. Boll Geofis Teor Appl 17:3–19

Emberson R, Kirschbaum D, Stanley T (2020) New global characterisation of landslide exposure. Nat. Hazards Earth Syst. 20(12):3413–3424. https://doi.org/10.5194/nhess-20-3413-2020

Ferrario MF, Livio F (2023) Rapid mapping of landslides induced by heavy rainfall in the Emilia-Romagna (Italy) region in May 2023. Remote Sens 16(1):122. https://doi.org/10.3390/rs16010122

Froude MJ, Petley DN (2018) Global fatal landslide occurrence from 2004 to 2016. Nat Hazards Earth Syst Sci 18(8):2161–2181. https://doi.org/10.5194/nhess-18-2161-2018

Gariano SL, Brunetti MT, Iovine GGR, Melillo M, Guzzetti F (2015) Calibration and validation of rainfall thresholds for shallow landslide forecasting in Sicily, southern Italy. Geomorphology 228:653–665. https://doi.org/10.1016/j.geomorph.2014.10.019

Gomes PI, Aththanayake U, Deng W, Li A, Zhao W, Jayathilaka T (2020) Ecological fragmentation two years after a major landslide: correlations between vegetation indices and geo-environmental factors. Ecol Eng 153:105914. https://doi.org/10.1016/j.ecoleng.2020.105914

Gozzini B, Giorgio B, Grifoni D (2022) The climate crisis and its impact on the territory, economic and social effects. Mod Environ Sci Eng 7(9):871–881. https://doi.org/10.15341/mese(2333-2581)/09.07.2021/001

Guzzetti F, Carrara A, Cardinali M, Reichenbach P (1999) Landslide hazard evaluation: a review of current techniques and their application in a multi-scale study, Central Italy. Geomorphology 31(1–4):181–216. https://doi.org/10.1016/S0169-555X(99)00078-1

Guzzetti F, Peruccacci S, Rossi M, Stark CP (2008) The rainfall intensity–duration control of shallow landslides and debris flows: an update. Landslides 5(1):3–17. https://doi.org/10.1007/s10346-007-0112-1

Guzzetti F, Mondini AC, Cardinali M, Fiorucci F, Santangelo M, Chang KT (2012) Landslide inventory maps: new tools for an old problem. Earth Sci Rev 112(1–2):42–66. https://doi.org/10.1016/j.earscirev.2012.02.001

Hölbling D, Eisank C, Albrecht F, Vecchiotti F, Friedl B, Weinke E, Kociu A (2017) Comparing manual and semi-automated landslide mapping based on optical satellite images from different sensors. Geosciences 7(2):37. https://doi.org/10.3390/geosciences7020037

Hürlimann M, Guo Z, Puig-Polo C, Medina V (2022) Impacts of future climate and land cover changes on landslide susceptibility: regional scale modelling in the Val d'Aran region (Pyrenees, Spain). Landslides 19(1):99–118. https://doi.org/10.1007/s10346-021-01775-6

Kushabaha A, Scardino G, Sabato G, Miglietta MM, Flaounas E, Monforte P, Scicchitano G (2024) ARCHIMEDE—an innovative Web-GIS platform for the study of medicanes. Remote Sens 16(14):2552. https://doi.org/10.3390/rs16142552

Lazzari M, Gioia D, Anzidei B (2018) Landslide inventory of the Basilicata region (Southern Italy). J Maps 14:348–356. https://doi.org/10.1080/17445647.2018.1475309

Masi EB, Bicocchi G, Catani F (2020) Soil organic matter relationships with the geotechnical-hydrological parameters, mineralogy and vegetation cover of hillslope deposits in Tuscany (Italy). Bull Eng Geol Environ 79(8):4005–4020. https://doi.org/10.1007/s10064-020-01819-6
Masi EB, Tofani V, Rossi G, Cuomo S, Wu W, Salciarini D, Catani F (2023) Effects of roots cohesion on regional distributed slope stability modelling. CATENA 222:106853. https://doi.org/10.1016/j.catena.2022.106853
Meena SR, Soares LP, Grohmann CH, Van Westen C, Bhuyan K, Singh RP, Catani F (2022) Landslide detection in the Himalayas using machine learning algorithms and U-Net. Landslides 19(5):1209–1229. https://doi.org/10.1007/s10346-022-01861-3
Mondini AC, Guzzetti F, Reichenbach P, Rossi M, Cardinali M, Ardizzone F (2011) Semi-automatic recognition and mapping of rainfall induced shallow landslides using optical satellite images. Remote Sens Environ 115(7):1743–1757. https://doi.org/10.1016/j.rse.2011.03.006
Mondini AC, Santangelo M, Rocchetti M, Rossetto E, Manconi A, Monserrat O (2019) Sentinel-1 SAR amplitude imagery for rapid landslide detection. Remote Sensing 11:760. https://doi.org/10.3390/rs11070760
Pawluszek K (2019) Landslide features identification and morphology investigation using high-resolution DEM derivatives. Nat Hazards 96(1):311–330. https://doi.org/10.1007/s11069-018-3543-1
Pellicani R, Spilotro G (2015) Evaluating the quality of landslide inventory maps: comparison between archive and surveyed inventories for the Daunia region (Apulia, Southern Italy). Bull Eng Geol Environ 74(2):357–367. https://doi.org/10.1007/s10064-014-0639-z
Peruccacci S, Brunetti MT, Luciani S, Vennari C, Guzzetti F (2012) Lithological and climatic control on rainfall thresholds for the possible initiation of landslides. Geomorphology 139:79–90. https://doi.org/10.1016/j.geomorph.2011.10.005
Plank S, Twele A, Martinis S (2016) Landslide Mapping in Vegetated Areas Using Change Detection Based on Optical and Polarimetric SAR Data Remote Sensing 8(4) 307–10.3390/rs8040307
Ramos-Scharrón CE, Arima EY, Hughes KS (2022) An assessment of the spatial distribution of shallow landslides induced by Hurricane María in Puerto Rico. Phys Geogr 43(2):163–191. https://doi.org/10.1080/02723646.2020.1801121
Report meteorologico Evento 2 novembre 2023 https://www.lamma.toscana.it/clima/report/eventi/evento_02112023.pdf
Salvatici T, Tofani V, Rossi G, D'Ambrosio M, Tacconi Stefanelli C, Masi EB, Casagli N (2018) Application of a physically based model to forecast shallow landslides at a regional scale. Nat Hazards Earth Syst Sci 18(7):1919–1935. https://doi.org/10.5194/nhess-18-1919-2018
Santangelo M, Althuwaynee O, Alvioli M, Ardizzone F, Bianchi C, Bornaetxea T, Fiorucci F (2023) Inventory of landslides triggered by an extreme rainfall event in Marche-Umbria, Italy, on 15 September 2022. Sci Data 10(1):427. https://doi.org/10.1038/s41597-023-02336-3
Smith HG, Spiekermann R, Betts H, Neverman AJ (2021) Comparing methods of landslide data acquisition and susceptibility modelling: examples from New Zealand. Geomorphology 381:107660. https://doi.org/10.1016/j.geomorph.2021.107660
Su Z, Chow JK, Tan PS, Wu J, Ho YK, Wang YH (2021) Deep convolutional neural network–based pixel-wise landslide inventory mapping. Landslides 18(4):1421–1443. https://doi.org/10.1007/s10346-020-01557-6
Swiss Re (2019), Natural catastrophes and man-made disasters in 2018: "secondary" perils on the frontline. Sigma No. 2/2019. https://www.swissre.com/institute/research/sigma-research/sigma-2019-02.html. Accessed 29 Jul 2025
Tao W, Jin H, Zhang Y (2007) Color image segmentation based on mean shift and normalized cuts. IEEE Trans Syst, Man, Cybern, Part B (Cybernetics) 37(5):1382–1389. https://doi.org/10.1109/TSMCB.2007.902249
Tavakkoli Piralilou S, Shahabi H, Jarihani B, Ghorbanzadeh O, Blaschke T, Gholamnia K, Aryal J (2019) Landslide detection using multi-scale image segmentation and different machine learning models in the higher Himalayas. Remote Sens 11(21):2575. https://doi.org/10.3390/rs11212575
Vai GB (2001) Structure and stratigraphy: an overview. *Anatomy of an Orogen: The Apennines and adjacent Mediterranean basins*, 15–31. https://doi.org/10.1007/978-94-015-9829-3
Valkaniotis S, Papathanassiou G, Marinos V, Saroglou C, Zekkos D, Kallimogiannis V, Ktenidou OJ (2022) Landslides triggered by medicane Ianos in Greece, September 2020: rapid satellite mapping and field survey. Appl Sci 12(23):12443. https://doi.org/10.3390/app122312443
Vannocci P, Segoni S, Masi EB, Cardi F, Nocentini N, Rosi A, Bicocchi G, D'Ambrosio M, Nocentini M, Lombardi L, Tofani V, Casagli N, Catani F (2022) Towards a national-scale dataset of geotechnical and hydrological soil parameters for shallow landslide modeling. Data 7(3):37. https://doi.org/10.3390/data7030037
Zeng T, Guo Z, Wang L, Jin B, Wu F, Guo R (2023) Tempo-spatial landslide susceptibility assessment from the perspective of human engineering activity. Remote Sens 15(16):4111. https://doi.org/10.3390/rs15164111

Publisher's Note Springer Nature remains neutral with regard to jurisdictional claims in published maps and institutional affiliations.

E. B. Masi (✉) · F. Caleca · P. Confuorto · V. Tofani · N. Casagli
Department of Earth Sciences, University of Florence, Via La Pira 4, 50121 Florence, Italy
Email: elenabenedetta.masi@unifi.it